HHS Public Access

Author manuscript

Curr Biol. Author manuscript; available in PMC 2020 March 04.

Published in final edited form as:

Curr Biol. 2019 March 04; 29(5): 790–802.e5. doi:10.1016/j.cub.2019.01.047.

Tulp3 regulates renal cystogenesis by trafficking of cystoproteins to cilia

Sun-Hee Hwang[#1], **Bandarigoda N. Somatilaka**[#1], **Hemant Badgandi**[1,4], **Vivek Reddy Palicharla**[1], **Rebecca Walker**[3], **John M. Shelton**[2], **Feng Qian**[3], and **Saikat Mukhopadhyay**[1,5,*]

[1]Department of Cell Biology, University of Texas Southwestern Medical Center, 5323 Harry Hines Boulevard, Dallas, TX 75390, USA

[2]Internal Medicine, University of Texas Southwestern Medical Center, 5323 Harry Hines Boulevard, Dallas, TX 75390, USA

[3]Division of Nephrology, University of Maryland School of Medicine, 655 West Baltimore Street, Baltimore, MD 21201, USA

[4]Present address: Department of Chemistry, Vanderbilt University, 7330 Stevenson Center, Nashville, TN 37235, USA

[5]Lead contact.

[#] These authors contributed equally to this work.

Summary

Polycystic kidney disease proteins, polycystin-1 and polycystin-2, localize to primary cilia. Polycystin knockouts have severe cystogenesis compared to ciliary disruption, whereas simultaneous ciliary loss suppresses excessive cyst growth. These data suggest the presence of a cystogenic activator that is inhibited by polycystins, and an independent but relatively minor cystogenic inhibitor, either of which are cilia-dependent. However, current genetic models targeting cilia completely ablate the compartment making it difficult to uncouple cystoprotein function from ciliary localization. Thus, the role of cilium-generated signaling in cystogenesis is unclear. We recently demonstrated that the tubby family protein Tulp3 determines ciliary trafficking of polycystins in kidney collecting duct cells, without affecting protein levels or cilia. Here, we demonstrate that embryonic stage nephron-specific *Tulp3* knockout mice developed cystic kidneys, while retaining intact cilia. Cystic kidneys showed increased MAPK/ERK, mTOR and persistently high cAMP signaling, suggesting contribution of multiple factors to cystogenesis. Based on kidney to body weight ratio, cystic index and epithelial proliferation in developing

[*]Correspondence: Saikat.Mukhopadhyay@utsouthwestern.edu (S. M.).

Author Contributions

S. M., S. H. H., and B. N. S. conceived the project, designed experiments, and analyzed data. S. H. H. and B. N. S. conducted most experiments. H. B. B. performed PC2 biochemistry experiments. V. P. P. identified Tulp3-dependent lipidated cargoes. J. S. S. helped with kidney histology. R. W. and F. Q. contributed PC2 trafficking reagents. S. M. wrote the paper with inputs from all authors.

Declaration of interests

The authors declare no competing interests.

tubules/cysts, the severity of cystogenesis upon *Tulp3* deletion was intermediate between that caused by loss of polycystin-1 or cilia. However, concomitant Tulp3 loss did not inhibit cystogenesis in polycystin-1 knockouts, unlike ciliary disruption. Interestingly, ciliary trafficking of the small GTPase Arl13b, loss of which causes cystogenic severity similar to ciliary loss, was reduced prior to cyst initiation. Thus, we propose that cystogenesis in *Tulp3* mutants results from a reduction of ciliary levels of polycystins, Arl13b, and Arl13b-dependent lipidated cargoes. Arl13b might be the ciliary factor that represses cystogenesis distinct from polycystins.

Graphical Abstract

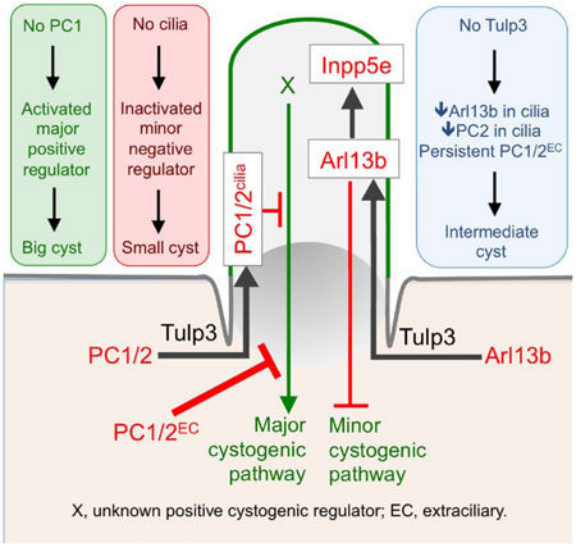

eTOC blurb

Hwang *et al.* show that embryonic stage nephron-specific *Tulp3* knockouts develop cystic kidneys, while retaining intact cilia. The severity of cystogenesis is intermediate between that caused by loss of polycystin-1 or cilia. They uncover evidence that cystogenesis results from a reduction of ciliary levels of polycystins and the small GTPase Arl13b.

Keywords

Tulp3; cilia; polycystic kidney disease; Arl13b; polycystin

Introduction

Primary cilia have now been established as sensory antennae in most vertebrate cells playing fundamental roles in cellular differentiation, polarity, and cell cycle control [1]. Multiple proteins that traffic to cilia, such as polycystin-1 and polycystin-2 (PC1/2, encoded by *PKD1/2*) [2, 3], fibrocystin [4, 5], and the small GTPase Arl13b [6, 7] have been implicated in cystic kidney disease, and are referred to as “cystoproteins”. In particular, PC1/2 belong to the TRP channel family of proteins, and PC2 functions as a non-selective cation channel in cilia [8-10]. Mutations in *PKD1/2* cause autosomal dominant polycystic kidney disease

(ADPKD) [11]. Another cystoprotein, Arl13b is an atypical member of the ADP-ribosylation factor-like (ARL) family of small G-proteins and is enriched in cilia [12]. It functions as a guanyl nucleotide exchange factor for Arl3 [13, 14] that determines trafficking of farnesylated [15] and myristoylated [16] proteins to cilia. Interestingly, lack of Arl13b-dependent ciliary cargoes, such as the farnesylated 5'phosphatase Inpp5e also causes kidney cystogenesis [17].

PC1/2 mostly reside in intracellular compartments, forming a complex in the endoplasmic reticulum before being trafficked to cilia [18-20]. Polycystin complex components are also shed in urinary exosomes [11, 21, 22]. The relative contribution of ciliary vs. extra-ciliary PC1/2 loss to cystogenesis is unclear. Based on PC1 [18, 23] and PC2 mutants that do not localize to cilia [18], ciliary pools of these proteins have been proposed to repress PKD pathogenesis. Extracellular polycystin domain mutants of *Pkd2* that do not traffic to nodal cilia also have defects in left-right asymmetry [24, 25]. However, as PC1/2 function is difficult to uncouple from ciliary localization, the role of ciliary pools needs to be reassessed by measuring channel activity of the wild type and mutant proteins in specific membrane microenvironments [8, 9], and in the context of protein maturation [18, 20, 23]. Thus, disrupting wild type PC1/2 localization to cilia would be the ideal approach for determining the relative contribution of their subcellular compartmentalization in PKD.

Compounding the challenges in determining the role of polycystins in ciliary compartment, the role of primary cilium in kidney cystogenesis is inherently complex and context-dependent. Whereas lack of nephron cilia [26], or cilia localized cystoproteins, such as Arl13b [6] or Inpp5e [17] results in cystic kidney disease, cystogenesis is less severe than upon *Pkd1/2* deletion [27, 28], Simultaneous *Pkd1/2* deletion and ciliary disruption partially or fully restores cystogenesis similar to loss of cilia alone, depending upon embryonic or adult-onset disease models, respectively [27]. Finally, the timing of ciliary loss is critical to the progression of cystogenesis [29-31]. Thus, the contribution of cilium-generated signaling in renal cystogenesis is not well understood.

We recently demonstrated that the tubby family protein Tulp3 determines ciliary trafficking of multiple proteins, including fibrocystin ciliary localization sequence containing chimeras, and PC1/2, without affecting respective protein levels or disrupting cilia [32, 33]. Here, using nephron-specific knockouts in mice, we identify Tulp3 as a suppressor of kidney cystogenesis by trafficking multiple cystoproteins to cilia, including polycystins and Arl13b.

Results

Lack of *Tulp3* causes cystic kidney disease

Tulp3 is expressed in the embryonic and early postnatal kidney by qRT-PCR (Figure S1A). Conditional *Tulp3* knockouts were generated using collecting duct-specific *HoxB7-Cre* (*HoxB7-Cre; Tulp3*$^{f/f}$) and nephron-specific *Ksp-Cre* (*Ksp-Cre; Tulp3*$^{f/f}$) [34, 35] (Figure S1B; hereafter referred to as *HoxB7-Tulp3* cko and *Ksp-Tulp3* cko, respectively). Both *Cre* lines exhibited kidney-specific knockdown of *Tulp3* (Figure S1C). Interestingly, both lines also exhibited a significant increase in the ratio between kidney to body weight, detected as early as postnatal day 10 (P10) (Figure 1A). By P24, *HoxB7-Tulp3* cko had significantly

increased kidney to body weight ratios ranging from 50-160 mg/g (Figure 1A), and renal cystic index ranging from ~70-85% (Figure 1B, S1D), along with elevated blood urea nitrogen (BUN) (Figure 1C). Similarly, *Ksp-Tulp3* cko had significantly increased but broader distribution of kidney to body weight ratio ranging from 10-170 mg/g (Figure 1A), renal cystic index (~20-80%) (Figure 1B), and BUN (Figure 1C). While *HoxB7-Tulp3* cko mice failed to survive beyond 1 month, *Ksp-Tulp3* cko mice survived till 2 months (Figure 1D). Further histological analysis suggested that *HoxB7-Tulp3* cko had extensive cysts throughout the kidneys with little remaining parenchyma at P24 (Figure 1E, Figure S1D). Most *Ksp-Tulp3* cko animals had extensive cysts at P24, while a few retained cortical parenchyma (Figure 1F, Figure S1D). Thus, lack of *Tulp3* results in kidney cystogenesis.

To confirm cyst origin, nephron segment-specific markers were used: Lotus tetragolonobus lectin (LTL) for proximal tubule, Tamm Horsfall protein (THP) for distal tubule/loop of Henle, and *Dolichos biflorus* agglutinin (DBA) or Aquaporin 2 (Aqp2) for collecting ducts. Consistent with *HoxB7-Cre* expression in the collecting duct, cysts in *HoxB7-Tulp3* cko were exclusively labeled with DBA/Aqp2 (Figure 2A, S2A). Consistent with high *Ksp-Cre* transgene expression in the distal nephron and collecting ducts [35], cysts in *Ksp-Tulp3* cko arose primarily from collecting ducts (DBA/Aqp2), occasionally from distal tubules (THP), but not from proximal tubules (Figure 2A, S2A).

Epithelial cell cilia lining *Tulp3* knockout cysts are unaffected

Cilia are intact upon embryonic or adult-onset conditional knockouts of polycystins [27, 28], However, nephron-specific or embryonic knockouts of *Arl13b* (*Ksp-Cre; Arl13b*$^{f/f}$ [6]; *Nestin-Cre; Arl13b*$^{f/f}$ [7]) lack cilia in collecting ducts postnatally, whereas there is a partial loss of cilia in the distal tubules and collecting ducts of conditional knockouts of the 5'phosphatase *Inpp5e* (*Ksp-Cre; Inpp5e*$^{f/f}$) [17]. However, the extent of ciliogenesis or length of cilia in collecting duct epithelial cells lining the cysts in either *Tulp3* cko model was unaffected even during advanced stages of cystogenesis at P24 (Figure 2B).

Increased ERK, mTOR and cAMP signaling in *Tulp3* conditional knockouts

Cyst formation in conditional knockouts of *Pkd1/2* [27, 28] or *Arl13b* [7] is associated with activation of components of the extracellular regulated kinase (MAPK/ERK) pathway. The ratios of phosphorylated ERK (pERK) and MEK (pMEK) to total levels of respective proteins in whole kidney lysates increased in either *Tulp3* cko cystic kidney model compared to control littermate kidneys at P24 (Figure 2C), and as early as P17 (Figure S2B).

Abnormal activation of mTOR signaling pathway has been implicated in cystic kidney disease caused by Ksp-Cre-mediated conditional knockout of *Inpp5e* [17]. *Nestin-Cre; Pkd1*$^{f/f}$ mice also show high mTOR pathway activity, but only around 1.5 months of age [36], whereas adult onset nephron-specific *Pkd1* conditional knockouts do not show increased mTOR signaling [27]. Elevated mTOR signaling is also a feature of late-onset cystic disease in a hypomorphic mutant of the IFT-B complex subunit *Ift88* [37]. At P24, the ratios of phosphorylated ribosomal protein S6 (pS6) to total S6 levels in whole kidney lysates were significantly increased in both *Tulp3* cko models compared to control littermates (Figure 2C) or *HoxS7-Cre*-mediated conditional knockout of *Pkd1* (Figure S2C).

Increased cAMP levels are present in cystic kidneys arising from either loss of PC2 [38] or cilia [39] during embryogenesis. In contrast, in adult-onset models of ADPKD, loss of PC1 induces increased cAMP levels at cystic stages, which is abrogated upon simultaneous ciliary disruption [27]. Reduction of renal cAMP levels also inhibits cystogenesis restoring kidney function in mouse models of ADPKD [40]. At P5, phosphorylated CREB (pCREB) was seen in nuclei of both *Tulp3* cko and control medullary cells (Figure S2D). However, at P24 pCREB persisted in nuclei of epithelial layers surrounding kidney cysts in *Tulp3* cko models, while being completely absent in control littermates (Figure 2D).

Overall, multiple downstream signaling pathways including ERK, mTOR and cAMP signaling are activated in *Tulp3* cko cystic kidneys, suggesting that multiple factors might contribute to cystogenesis.

Cystogenesis in *Tulp3* conditional mutants is less severe than upon *Pkd1* deletion

We next compared the severity of cystogenesis in *Tulp3* conditional knockouts compared to loss of *Pkd1* or cilia. Cysts in both *HoxB7-Tulp3* cko and *Ksp-Tulp3* cko were apparent by P5, and mostly affected the outer medulla (Figure 3Aa-c, 3B-C). Similarly, *HoxB7-Cre; Ift88*$^{fl/fl}$ (*HoxB7-Ift88* cko), which lacked cilia by P5 in collecting duct epithelia (Figure S3A), also exhibited outer medullary cysts at P5 (Figure 3Ad, 3B-C). However, by P24, the *HoxB7-Tulp3* cko kidneys were significantly larger and had higher cystic index than *HoxB7-Ift88* cko kidneys (Figure 3D-E). Double conditional knockouts of *Tulp3 and Ift88* with *HoxB7-Cre* (*HoxB7-Tulp3; Ift88* dko) lacked cilia in cysts (Figure S3A) and were grossly similar to the *Ift88* single conditional knockouts in having mostly medullary cysts at P5 (Figure 3Ae, 3B-C). No significant differences were seen between the *HoxB7-Tulp3; Ift88* dko and *Ift88* single conditional knockout kidneys at P24 (Figure 3D-E). In contrast, *HoxB7-Cre; Pkd1*$^{f/f}$ (*HoxB7-Pkd1* cko) cysts, which retain cilia (Figure S3A), were distinctively larger in size and had higher cystic index at P5 and P24 than *HoxB7-Tulp3* cko (Figure 3B-E). Cysts were present in *HoxB7-Pkd1* cko animals throughout the kidney parenchyma by P5 (Figure 3Af). Thus, cystogenesis upon *Tulp3* deletion was slower to develop similar to ciliary disruption, while being more severe than loss of cilia at later stages. Cystogenesis upon *Tulp3* deletion was much less severe than that caused from loss of PC-1 at all stages.

Increased proliferation in cystic kidneys in *Tulp3* conditional knockouts with respect to loss of cilia

Increased proliferation has been linked to kidney-specific murine knockouts of *Pkd1/2* [27, 28]. However, proliferation rates decrease with cyst progression in *Pkhd1-Cre; Pkd1*$^{f/-}$ mice [28]. To mechanistically differentiate between the developmental stages of cysts, proliferation rates in kidneys of single and double conditional mutants of *Tulp3, Ift88* and *Pkd1* were determined by measuring BrdU incorporation after an acute pulse. At P5, many of the cysts in *HoxB7-Pkd1* cko were lined by squamoid cells without Aqp2 immunostaining (Figure S3C). Although, the combined proliferation rate in all cysts in *HoxB7-Pkd1* cko was not different from control animals (Figure 3F), Aqp2-negative cysts had significantly higher proliferation rates compared to Aqp2-positive areas (Figure 3F). Proliferation also increased in the collecting duct epithelia of both *Tulp3* conditional

knockout models with respect to control littermates at P5, and remained high at P24 even after declining from P5 levels, compared to controls with no proliferation (Figure 3F, S3B-D). Interestingly, proliferation was significantly higher in collecting duct cells of *HoxB7-Tulp3* cko with respect to *HoxB7-Ift88* cko at P5 (Figure 3F, S3C), although cystic index was not different at P5 (Figure 3C). Thus, *Tulp3* conditional knockouts have higher proliferation with respect to loss of cilia.

Lack of *Gpr161* does not cause cystic kidney disease

We next set out to identify which of the Tulp3-regulated ciliary cargoes [32, 33, 41] might be responsible for the *Tulp3* cko phenotypes. We previously demonstrated that Tulp3 determines trafficking of the orphan GPCR, Gpr161 to cilia in the kidney IMCD3 cell line [41]. We determined that *Gpr161* was expressed in the kidney during embryogenesis and postnatally, by radioisotopic RNA *in situ* hybridization and qRT-PCR, respectively (Figure 4A-B). Despite kidney-specific *Gpr161* deletions (Figure 4C), neither the ratio between kidney to body size nor BUN levels were altered relative to controls (Figure 4D-E). Histological analysis suggested that kidneys were not cystic (Figure 4F), although Gpr161 localization to cilia of cultured primary collecting duct cells isolated from medulla of *Ksp-Tulp3* cko kidneys at P20 was affected (Figure S4A-B; Methods). Thus, Gpr161 trafficking to cilia is not a critical factor in restricting cystogenesis.

PC2 ciliary trafficking is decreased in *Tulp3* knockout primary collecting duct cells

We previously demonstrated the lack of stably expressed PC1 and endogenous PC2 trafficking to cilia in collecting duct cell lines upon *Tulp3* RNAi [33]. As we were unable to immunostain for PC2 in kidney sections, we tested for PC2 trafficking in primary collecting duct cells isolated from medulla of control, *Ksp-Tulp3* cko and *HoxB7-Tulp3* cko kidneys at P20 and P16, respectively (Figure S4A; Methods) [42]. Cells were cultured in media supplemented with dibutryl cAMP, as increased cAMP signaling causes Aqp2 phosphorylation and trafficking from intracellular vesicles to the plasma membrane [42], allowing identification of collecting duct epithelial cells by Aqp2 immunostaining. *Tulp3* transcript levels were completely absent in the cko cells, as detected by qRT PCR. Ciliation or ciliary Ift88 levels were not affected in collecting duct epithelial cells from both cko models. However, PC2-positive cilia were dramatically reduced compared to control in either model, whereas ER pools remained unaffected (Figure 5A-B, Figure S5A-B). Thus, PC2 trafficking to cilia is impaired in *Tulp3* knockout primary collecting duct cells.

PI(4,5)P_2-dependent PC2-TULP3 interactions

We previously demonstrated that trafficking of $PC2^{703X}$lacking the C-tail, which does not require PC1 for trafficking to cilia [43, 44], is affected upon *Tulp3* knockdown [33]. To further probe if PC2 is in close proximity to TULP3, we assayed for proximity biotinylation of $PC2^{703X}$ tagged at its C-terminus with LAP (S tag-PreScission-GFP) upon co-expressing a promiscuous biotin protein ligase-tagged TULP3 (BirA*-Tulp3; BirA*, biotin protein ligase mutant R118G) [45]. We used $^{SNAP}Gpr161^{LAP}$ and $^{SNAP}Smo^{LAP}$ as positive and negative controls for proximity to TULP3, respectively [33, 46]. After incubating the transfected cells with biotin, we checked for cumulative biotinylation in the immunoprecipitates (Figure S5C, Methods). We detected significant biotinylation in both

PG2^{703X} and Gpr161, compared to Smo (Figure S5C). Mutations in the tubby domain of TULP3 that contribute to PI(4,5)P_2 binding (TULP3$^{K268A;\ R270A}$) [32, 47] reduced the levels of biotinylated PC2^{703X} similar to Smo transfection (Figure S5C). In addition, a N-terminal deleted mutant Δ(5-72 aa) of PC^{L703X} ($^{\Delta NT}$PC2^{703X}) that does not localize to cilia (Figure S5D) [43] but traverses Golgi (Figure S5E) had reduced biotinylation with TULP3, which further reduced with TULP3$^{K268A;\ R270A}$ (Figure S5C). Thus, TULP3 and PC2^{703X} are in close proximity in a PI(4,5)P_2-dependent manner.

Concomitant loss of *Tulp3* does not inhibit cystogenesis of *Pkd1* deleted animals

Based on cystic index and proliferation in developing tubules and cysts, the severity of cystogenesis from *Tulp3* deletion was intermediate between *Pkd1* deletion and ciliary disruption. We thus compared the progression of cystogenesis in *HoxB7-Cre*; *Pkd1*$^{f/f}$ *Tulp3*$^{f/f}$ (*HoxB7-Pkd1*; *Tulp3* dko) with respect to *HoxB7-Pkd1* cko and *HoxB7-Tulp3* cko. We noted that *HoxB7-Pkd1*; *Tulp3* dko mice had higher kidney to body weight ratios at P5 and were lethal by P20 (as we never recovered double knockouts after P18) compared to *HoxB7-Pkd1* cko, which still survived at least till P24 (Figure 5C-E). Similarly, the *HoxB7-Cre*; *Pkd1*$^{f/f}$; *Tulp3*$^{f/+}$ animals had higher kidney to body weight ratios compared to *HoxB7-Pkd1* cko at P5. However, cystic indices of these three strains were not different from each other at either P5 or P18-24 (Figure 5C-E, S5F). The kidney to body ratios or cystic indices of *HoxB7-Cre*; *Pkd1*$^{f/+}$; *Tulp3*$^{f/f}$ mice were not different from *HoxB7-Tulp3* cko ruling out effects upon partial loss of PC-1 (Figure 5C-E, S5F). Thus, concomitant loss of *Tulp3* does not inhibit the cystogenic phenotype of *Pkd1* deletion, unlike disruption of cilia. Rather, complete or partial loss of Tulp3 in polycystin knockouts is earlier lethal and/or quicker in developing enlarged kidneys than *HoxB7-Pkd1* cko, while having similar extent of cystogenesis. These results suggest that at least some of Tulp3 functions in the kidney are independent of Pkd1.

Defective ciliary trafficking of Arl13b precedes cyst initiation in *Tulp3* cko models

Given that cilia from epithelial cells lining the cysts in *Tulp3* conditional mutants are not affected during cyst initiation or at later stages (Figure 2B, 6A-B, S4A), defective ciliary trafficking of proteins in addition to PC2 might account for the intermediate cystic disease phenotypes in these mice. One candidate is the small GTPase Arl13b, because of its role in causing cystogenesis [6, 7], similar in timeline and extent of cystogenesis compared to loss of cilia or Tulp3 ([6, 26] and this study, by comparing *Ksp-Cre* cko models). Trafficking of Arl13b to cilia was dramatically reduced in *HoxB7-Tulp3* cko or *Ksp-Tulp3* cko collecting duct epithelia, thus identifying Arl13b as a potential Tulp3-dependent cargo. Interestingly, this defect was evident as early as P0, well before cysts were apparent in either model. (Figure 6A-B, S6A). Adjacent Aqp2-negative nephron segments still retained Arl13b-positive cilia at these stages, confirming that the trafficking defect is primarily in collecting ducts. Trafficking of Arl13b to cilia was unaffected in *HoxB7-Pkd1* cko cysts (Figure S6B). Thus, lack of Arl13b trafficking to cilia precedes cyst formation in *Tulp3* cko models.

Defective trafficking of Arl13b-regulated lipidated cargo Inpp5e in *Tulp3* cko cysts

Lack of the Arl13b-dependent ciliary cargo Inpp5e also causes kidney cystogenesis [17], similar in timeline and extent of cystogenesis compared to loss of cilia or Tulp3 ([17, 26],

and this study, by comparing *Ksp-Cre* cko models). Inpp5e was localized to cilia of collecting duct epithelial cells (Figure 7A, S5A), whereas it was diffusely localized to the cytoplasm in Aqp2-negative tubules with weak to no ciliary localization (Figure S5A-B). Interestingly, ciliary trafficking of Inpp5e was also reduced in either *HoxB7-Tulp3* cko or *Ksp-Tulp3* cko cysts by P5, although ciliary pools were only marginally reduced at P0 before cyst initiation (Figure 7A-B, S5A). Thus, Arl13b depletion in collecting duct cilia causes a gradual defect in ciliary transport of Inpp5e.

Discussion

Nephron-specific *Tulp3* knockouts in mice result in kidney cystogenesis without disrupting cilia. A hypomorphic mutation of *Tulp3* also causes kidney cystogenesis without disrupting cilia (Karel Liem, personal communication). Multiple downstream signaling pathways including MAPK/ERK, mTOR and cAMP signaling were elevated in the cystic kidneys induced upon *Tulp3* knockdown, suggesting that dysregulation of multiple signaling pathways contribute to cystogenesis. Furthermore, based on kidney to body weight ratio, cystic index and epithelial proliferation in developing tubules and cysts, the severity of cystogenesis upon *Tulp3* deletion was intermediate between that caused by loss of polycystin-1 or cilia. Given the role of Tulp3 in trafficking of multiple cystoproteins to cilia of collecting duct epithelial cells, including polycystins and Arl13b, we propose that kidney cystogenesis in the *Tulp3* conditional knockout models resulted from cumulative effects of lack of localization of multiple cystoproteins without affecting ciliogenesis. The expanding role of Tulp3 in determining composition of the ciliary lipidome, by functioning as a master regulator for Arl13b and Arl13b-regulated lipidated cargo trafficking to cilia is an important focus of our current studies.

Grossly, the extent of cystogenesis in *Tulp3* conditional mutants, and the timeline for cyst development paralleled that of (a) collecting duct-specific knockouts of the IFT-A complex (*HoxB7-Cre: Ift140*$^{f/null}$) [48] and IFT-B complex (*HoxB7-Cre: Ift20*$^{f/null}$) [49], both of which disrupt cilia, (b) nephron-specific knockouts of *Arl13b* (*Ksp-Cre; Arl13b*$^{f/f}$) [6], *Inpp5e* (*Ksp-Cre; Inpp5e*$^{f/f}$) [17] and germline knockouts of *Arl3* [50]. Defective trafficking of Arl13b to cilia was clearly apparent even before initiation of cystogenesis in *Tulp3* cko models. Thus, lack of Arl13b in cilia might be the major contributor to cystogenesis from *Tulp3* depletion. The apparent lack of ciliary defects in *Tulp3* cko models despite absence of Arl13b in cilia in comparison to *Arl13b* conditional knockout models [6, 7] might arise from milder effects from undetectable or gradual loss of ciliary Arl13b, or extra-ciliary function of Arl13b in ciliary maintenance.

Cystogenesis induced upon PC1/2 loss is more severe than that occurring upon ciliary disruption, whereas concomitant loss of cilia in *Pkd1/2* conditional knockouts suppresses cyst growth [27]. The most parsimonious model explaining these data posits the presence of positive regulator/s and relatively minor negative regulator/s of cystogenesis, both of which are cilia-dependent [51]. The positive regulator of cystogenesis is inhibited by PC1/2; however, this factor functions independently of the minor negative regulator/s (Figure 7C) [27, 51]. Based on our results that cystogenesis upon *Tulp3* deletion was slow to develop

similar to that upon ciliary disruption or Arl13b loss, Arl13b might be the cilia localized negative regulator of cystogenesis that functions independent of PC1/2 (Figure 7C).

Concomitant loss of Tulp3 does not inhibit the cystogenic phenotype of *Pkd1* deletion, unlike loss of cilia (where both the positive and negative cystogenic regulators are lost). Rather, the *HoxB7-Pkdf, Tulp3* dko is earlier lethal and quicker in developing enlarged kidneys than *HoxB7-Pkd1* cko, while having similar extent of cystogenesis. The positive cystogenic ciliary regulator persists while the minor negative cystogenic ciliary regulator is removed from loss of both PC1 and Tulp3 (Figure 7C). Increased cystogenesis upon Tulp3 loss compared to loss of cilia could result from limited activation of the cilia-dependent major cystogenic pathway from lack of ciliary PC1/2 pools (Figure 7C). Extra-ciliary pools of PC1/2 could contribute in restricting the positive regulator of cystogenesis in *Tulp3* cko models (Figure 7C), explaining such partial activation. Alternatively, PC1/2 depletion from cilia upon *Tulp3* deletion could be temporally delayed compared to early Arl13b loss.

The effect of Arl13b depletion on cilia might result from a gradual defect of ciliary transport of lipidated cargoes, particularly of the farnesylated protein Inpp5e in the collecting duct [15]. In agreement with this model, *Ksp-Cre*-mediated deletion of *Inpp5e* results in severity of cystogenesis [17] similar to that upon *Arl13b* deletion [6] and ciliary disruption [26], and hyperactivation of mTOR pathway [17]. We cannot however rule out the effects of gradual loss of other lipidated cargoes, including the myristoylated Nphp3 [16] upon loss of Arl13b trafficking to cilia, particularly at later stages of cyst progression in adults and in other tubule segments [52]. Future work would need to address the role of these individual ciliary cargoes in kidney cystogenesis in *Tulp3* mutants.

STAR Methods

CONTACT FOR REAGENT AND RESOURCE SHARING

Further information and requests for resources and reagents should be directed to and will be fulfilled by the Lead Contact, Saikat Mukhopadhyay (saikat.mukhopdahyay@utsouthwestern.edu).

EXPERIMENTAL MODEL AND SUBJECT DETAILS

ES cells—ES cells targeting the second exon of *Tulp3* from EUCOMM (HEPD 0508-5-B01) were used to generate the floxed mice and were obtained from MRC, Harwell. ES cells were grown on SNL feeders with media containing 20% serum, 6 mM L-glutamine, 1× penicillin/streptomycin, 1 mM β-mercaptoethanol, 1 mM Non-essential Amino Acids, 1× nucleosides, 10 mg/L sodium pyruvate, ESGRO Leukemia Inhibitory Factor (LIF) supplement (10^7 units/ml) 66 μl/L, and incubated at 37°C in 5% CO_2.

Mice—All mice were housed at the Animal Resource Center of the University of Texas Southwestern (UTSW) Medical Center. All protocols were approved by the UTSW Institutional Animal Care and Use Committee. Mice were housed in standard cages that contained three to five mice per cage, with water and standard diet *ad libitum* and a 12 hour light/dark cycle. Both male and female mice were analyzed in all experiments. *HoxB7-Cre* and *Ksp-Cre* mice were obtained from O'Brien Kidney Research Core of UT Southwestern.

ES cells targeting the second exon of *Tulp3* from EUCOMM (HEPD 0508-5-B01) were used to generate the floxed mice that were obtained from MRC, Harwell for this study. We did not notice any difference between wild type or heterozygous animals for *Tulp3* floxed alleles with or without *Cre* recombinase, and thus were all included as littermate controls as mentioned in respective figure legends. *Ift88*$^{f/f}$ (*B6.129P2-Ift88*^{tm1Bky}*/J*; Stock No. 022409) mice were obtained from Jackson Laboratory (Bar Harbor, ME). *Pkd1* floxed mice were obtained from O'Brien Kidney Research Core, UT Southwestern. We generated a new mouse allele of *Gpr161* that was floxed on both sides of exon 4 allowing conditional deletion for studying tissue-specific phenotypes [53, 54]. By generating embryos homozygous for global deletion, we determined the knockout embryos to have craniofacial defects, neural tube defects and ventralization [53], similar to the previous null allele targeting exon 3 [41]. Thus, the present floxed allele upon recombination results in a null allele. The *Gpr161* floxed mouse strains were maintained in a C57BL/6 background. To assess the rate of cell division we administered a pulse of BrdU (B5002; Sigma; 50 mg of BrdU/kg body mass dissolved in PBS) injected intraperitoneally 3 h before the mice were sacrificed for analysis. Pups of ages P0 to P24 were analyzed for renal cysts as mentioned in the figure legends.

Primary kidney collecting duct cell cultures

Primary kidney collecting duct cell cultures were performed according to published methods [42]. P20 *Ksp-Cre; Tulp3 cko* mice or control littermates and P16 *HoxB7-Cre; Tulp3 cko* mice or control littermates were decapitated and bled. Kidneys were removed and washed in sterile DPBS (supplemented with 0.25 μg/ml gentamicin (345814-M; Sigma) and nystatin (N1638; Sigma); DPBS-GN) on ice. Next steps were carried out in a sterile workstation. Kidneys were transferred onto a sterile compress to remove excessive liquid and the fatty kidney capsule was removed with sterile forceps. Kidneys were bisected and the whitish inner medullae were dissected. Medullae were transferred into sterile enzyme solution containing 1 mg/ml hyaluronidase (H6254; Sigma) and 2.2 mg/ml collagenase (NC9460908; Worthington/Fisher) in DPBS-GN (1 ml of enzyme solution/ 2 kidney inner medullae). Inner medullae suspension was incubated at 37 °C for 1 hour with continuous shacking. The suspension was triturated with a blunted glass Pasteur pipette until it became homogeneously turbid. Suspension was centrifuged for 5 min at 300 × g at 16 °C. The supernatant was discar ded and the pellet was resuspended thoroughly in DPBS-GN and re-centrifuged. Cells were resuspended in complete medium [DMEM (D5796; Sigma), 1% non-essential amino acids (M7145; Sigma), 1% FBS (F6178; Sigma), 500 μM dibutryl cAMP (D0627; Sigma), 20 U/ml nystatin and 0.25 μg/ml gentamicin] and seeded in collagen IV (C6745; Sigma) coated 6 cm culture dishes with or without loosely attached collagen IV coated cover slips. During the next week the cells were washed 2 times with complete medium. 6-7 days after seeding, the kidney collecting duct cells on coverslips were starved for 48 hours (0.2% FBS, and dibutryl cAMP) and fixed with 4% paraformaldehyde (15710; Electron microscopy solutions) at 37°C for 10 min to perform immunofluorescence experiments. Cells in 6 cm culture dishes without coverslips were pelleted and frozen at the same time for qRT-PCR. The cultures were repeated four times for *Ksp-Cre; Tulp3 cko* mice and thrice for *HoxB7-Cre; Tulp3 cko* mice.

METHOD DETAILS

Mouse genotyping—For genotyping of *Tulp3*$^{f/f}$ mice, we used the following primers: (a) Tulp3-5'Cas-WTF (5' CCA TTT GTG AGG GTT GCT TT 3') and Tulp3-Crit-WTR (5' GCT AAC ACA AGC CCA TGC TA 3') to detect wild type band (256bp) and floxed band (450 bp), and (b) Tulp3-F1 (5' AAG GCG CAT AAC GAT ACC AC 3') and Tulp3-R1 (5' ACT GAT GGC GAG CTC AGA CC 3') to detect the deletion. For genotyping *Ift88,* following primers were used to detect mutant (410 bp) and wild type band (365 bp): 16967-F (5'-GAC CAC CTT TTT AGC CTC CTG-3'), 16969-R (5'-AGG GAA GGG ACT TAG GAA TGA-3'). For genotyping *Pkd1* floxed allele, following primers were used to detect mutant (400 bp) and wild type band (200 bp): Pkd1-F (5'- CCG CTG TGT CTC AGT GTC TG-3'), Pkd1-R (5'- CAA GAG GGC TTT TCT TGC TG-3'). For genotyping Cre, following primers were used to detect transgene band: Cre-F (5' AAT GCT GTC ACT TGG TCG TGG C 3'), Cre-R (5' GAA AAT GCT TCT GTC CGT TTG C 3'). For genotyping of *Gpr161*$^{f/f}$ mice, following primers were used to detect wild type band (816bp), flox band (965 bp) and deleted band (340bp); P1 (5' CAA GAT GGA TTC GCA GTA GCT TGG 3'), P2 (5' ATG GGG TAC ACC ATT GGA TAC AGG 3'), and P3 (5' CAA CGG GTT CTT CTG TTA GTC C 3').

Tissue processing, antibodies, immunostaining and microscopy—Mice were perfused with PBS, and the kidneys were dissected and fixed in 4% paraformaldehyde overnight at 4°C, and processed fo r cryosection or paraffin embedding and sectioning. For cryosection, the kidneys were incubated in 30% sucrose for 1-2 days at 4°C. Kidneys were mounted with OCT compound, and cut into 15 μm frozen sections. For paraffin section, kidneys were processed over a 12-hour period using a Thermo-Fisher Excelsior Automated Tissue Processor (A82300001; ThermoFisher Scientific), which dehydrated the kidneys through 6 ethanol concentrations, from 50% ethanol to 100% ethanol, cleared through 3 changes of xylene, and infiltrated with wax through 3 Paraplast Plus paraffin baths (39602004; Leica). Samples were embedded in Paraplast Plus using paraffin-filled stainless steel base molds and a Thermo-Shandon Histocenter 2 Embedding Workstation (6400012D; ThermoFisher Scientific). The kidneys were then cut in 5 μm thick sections, deparafinned and treated with microwave in Antigen Retrieval citra solution (HK086-9K; BioGenex, Fremont, CA) for 10 min. For frozen sections, the sections were incubated in PBS for 15 min to dissolve away the OCT. Sections were then blocked in blocking buffer (1% normal donkey serum [Jackson immunoResearch, West Grove, PA], in PBS) for 1 hour at room temperature. Sections were incubated with primary antibodies against the following antigens; overnight at room temperature or 4C: Acetylated tubulin (1:500, T6793; Sigma mouse IgG2b) Arl13b (1:500, N295B/66; NeuroMab Facility), BrdU (1:500, ab6326; Abeam), Aqp2 (1:500 A7310 Sigma rabbit polyclonal; SC515770, Santa Cruz Biotechnology mouse IgG1), pCREB (1:500, 9198S Cell Signaling), Inpp5e (17797-1-AP; Proteintech). Anti-PC2 affinity purified rabbit polyclonal was a gift from Dr. Gregory Pazour (UMass Medical School) [33]. For BrdU staining, sections were treated with 2 N HCl for 15 min at 37°C and washed before incubating with blocking buffer. After three PBS washes, the sections were incubated in secondary antibodies (Alexa Fluor 488-, 555-, 594-, 647- conjugated secondary antibodies, or anti-mouse IgG isotype-specific secondary antibodies; 1:500; Life Technologies, Carlsbad, CA or Jackson ImmunoResearch) or cell

surface markers, Fluorescein labeled Dolichos Biflorus Agglutinin (DBA; 1:200, FL 1031 Vector laboratories), Anti-Tamm Horsfall Glycoprotein antibody (THP; 1:60, BT 590, Biomedical Technologies Inc.) for 1 hour at room temperature. Cell nuclei were stained with DAPI (Sigma) or Hoechst 33342 (Life technologies). Slides were mounted with Fluoromount-G (0100-01; Southern Biotech) and images were acquired with a Zeiss Axiolmager.Z1 microscope and a Zeiss LSM780 confocal microscope. For hematoxylin and eosin staining, paraffin sections were stained by hematoxylin and eosin (Hematoxylin 560; 3801575; Leica and Alcoholic Eosin Y 515; 3801615; Leica) using a Sakura DRS-601 x-y-z robotic-stainer (DRS-601; Sakura-FineTek, Torrance, CA). Slides were dehydrated and mounted with Permount (SP15-100; ThermoFisher Scientific). Immunofluorescence experiments were replicated with multiple mice or kidneys as indicated in the respective figure legends. No blinding was performed. Sample sizes were based on our experience with these assays. Each dot represents data from a separate mouse or kidney as shown in figures.

Quantitative RT-PCR—RNA samples were derived from kidneys of Cre-positive floxed mice and littermate controls. RNA was extracted using the GenElute mammalian total RNA purification kit (RTN350; Sigma). Genomic DNA was eliminated by DNase I (D5307; Sigma). cDNA was synthesized by iScript (1708890; Bio-Rad) or M-MLV Reverse Transcriptase (M1427; Sigma). qRT-PCR was performed with Kicqstart One-Step Probe RT-qPCR ReadyMix (KCQS07; Sigma). Single Tube Taqman Gene Expression Assays were used for *Tulp3* (Mm00495808_m1), *Gapdh* (Mm99999915_g1) and *Gpr161* (MM01291057_M1). Reactions were run in CFX96 thermocycler (Bio-Rad). qRT-PCR for each RNA sample was done with at least 2 technical replicates.

***In situ* hybridization—**Both antisense and sense radiolabeled riboprobes for *Gpr161* were synthesized *in vitro* according to the manufacturer's specifications (Ambion) and labeled with ^{35}S-UTP (>1,000 Ci/mmol; NEG039H, PerkinElmer LAS Canada, Inc.). Tissues were cut into 9 μm sections and mounted on Superfrost® Plus slides (Fisher Scientific, 12-550-15). Before ISH, sections were fixed in 4% PFA in PBS, treated with triethanolamine/acetic anhydride, washed and dehydrated in a series of ethanols. Sections were hybridized overnight at 55°C in 50% deionized formamide, 0.3 M NaCl, 20mM Tris-HCl pH 7.4, 5 mM EDTA, 10 mM NaH_2PO_4, 10% dextran sulphate, 1X Denhardt's, 50 μg/ml total yeast RNA, and 50-80,000 cpm/μl ^{35}S-labeled cRNA probe. The tissues were subjected to stringent washing at 65°C in 50% formamide, 2X SSC, 10 mM DTT and washed in PBS before treatment with 20 μg/ml RNAse A at 37°C for 30 minutes. Following washes in 2X SSC and 0.1X SSC for 10 minutes at 37°C, the slides were dehydrated and exposed to Kodak BioMaxMR x-ray film for 4 days then dipped in Kodak NTB nuclear track emulsion and exposed in light-tight boxes with desiccant at 4°C for 17 days. Photographic development was carried out in Kodak D-19 [54]. Sections were counterstained lightly with cresyl violet and analyzed using brightfield and darkfield microscopy. Sense (control) riboprobes established the level of background signal.

Cystic index quantification—Cystic index was quantified in paraffin embedded mid-sagittal sections of whole kidneys. HE stained kidney sections were photographed by the PrimeHisto XE slide scanner (Pacific Imaging, Inc.) using HistoView Software. ImageJ

software (National Institutes of Health, Bethesda, MD) was used to calculate the cystic index. The images were converted to 8-bit grey scale. Equal sized non-overlapping areas were cropped covering the entire kidney image. The image threshold was adjusted similarly, and the percentage of black area was analyzed in each cropped image. Data from all cropped areas from the kidney were averaged and finally subtracted from 100 to give the cystic index as a percent. Sample sizes were based on our experience with these assays. No data was excluded. Each dot represents data from a separate kidney as shown in figures.

BUN measurement—Mice were euthanized and blood samples were obtained by ventricular puncture. BUN measurements were obtained using the Vitros 250 chemistry analyzer (GMI Inc., Ramsey, MN). Sample sizes were based on our experience with these assays. No data was excluded. Each dot represents data from a separate mouse as shown in figures.

Proximity biotinylation experiments—T-REx-293 cells were cotransfected with 5-7.5 μg each of indicated constructs. The media was supplemented with 20 μM biotin for 12 h before harvesting using PBS with 2 mM EDTA 2mM EGTA 48 h post transfection. Cells were lysed in 50 mM Tris-HCl, pH 7.4, 200 mM KCl, 1 mM MgCl2, 1mM EGTA, 10 % glycerol, 1 mM DTT, 1% digitonin, 0.05% n-Dodecyl-β-D-Maltoside, 0.25% Cholesteryl hemisuccinate, 1 mM of AEBSF, 0.01 mg/mL of Leupeptin, pepstatin and chymostatin [55]. Lysates were centrifuged at 12000×g for 10 min followed by tandem IPs (Figure S5C). Briefly, the GFP immunoprecipitates were first digested with PreScission protease for 16 h at 4°C. The supernatants were split to two aliquots and subjected to secondary IPs with S-protein agarose and Neutravidin, respectively [33]. The resulting secondary IPs were lysed in urea sample buffer [55], and analyzed by Western blotting. Blots were probed with antibodies against S tag, Flag followed by visualization using IRDye tagged secondary antibodies. IRdye tagged neutravidin was used for detecting biotinylation signal on blots.

QUANTIFICATION AND STATISTICAL ANALYSIS

To assess ciliation, at least two different fields in the medullary and cortical regions from N=2/3 mice at each age were imaged with the 63x objective in a LSM780. Total number of acetylated tubulin (AcTub) positive cilia in Aqp2 positive cells were expressed as a percentage. Length of >100 cilia/mouse of each genotype was measured using ImageJ software (National Institutes of Health, Bethesda, MD). To quantifiy BrdU positive collecting duct cells five different fields from separate kidneys were imaged with the 40x objective in a LSM780 or 10x in a Zeiss AxiolmagerM1. Cells positive for BrdU among Aqp2 expressing tubules/cysts were averaged per mouse. To quantify PC2 positive ciliated collecting duct primary kidney collecting duct cells, 5 different fields in a coverslip of cells cultured from each mice at P20 were imaged with the 63x objective in a LSM780. Cells positive for Aqp2 and AcTub both were averaged per mouse as ciliated cells. Cells positive for Aqp2, AcTub and PC2 were averaged per mouse as PC2 positive ciliated cells. To quantify Arl13b/Inpp5e positive ciliated collecting duct cells 2-5 different fields in the medullary and cortical regions from each mice at each age were imaged with the 63x objective in a LSM780. Cells positive for Aqp2 and AcTub both were averaged per mouse as ciliated cells. Cells positive for Aqp2, AcTub and Arl13b/Inpp5e were averaged per mouse

as Arl13b/Inpp5e positive ciliated cells. All data in Figures are expressed as mean ± SD or SEM. To determine the statistical significance of differences among genotypes we performed one-way ANOVA with Sidak's multiple comparisons tests, or unpaired, two-sided, student's *t* tests that assumed unequal variances in treatments, as mentioned in legends. Microsoft Excel and GraphPad Prism (GraphPad, La Jolla, CA) were used for statistical analysis. Values of $P<0.05$ were considered significant.

Supplementary Material

Refer to Web version on PubMed Central for supplementary material.

Acknowledgements

We thank Karel Liem for sharing unpublished data on a *Tulp3* allele with cystic kidney disease. This work was supported by a recruitment grant from CPRIT (R1220 to S.M.), R01 grants from NIH (1R01GM113023, S.M.; R01DK111611, F.Q.), a pilot and feasibility grant from O'Brien Kidney Center (P30DK079328, NIDDK) to S. M., and support from the Baltimore PKD Research Center (P30DKO90868, NIDDK). We thank the Mouse Transgenic Core, UT Southwestern. We thank Peter Igarashi, Thomas Carroll, Gregory Pazour, Dennis Marciano, and Tamara Caspary for reagents, and Sandra Schmid, Karel Liem, and anonymous reviewers for comments on the manuscript.

References

1. Goetz SC, and Anderson KV (2010). The primary cilium: a signalling centre during vertebrate development. Nat Rev Genet 11, 331–344. [PubMed: 20395968]
2. Pazour GJ, San Agustin JT, Follit JA, Rosenbaum JL, and Witman GB (2002). Polycystin-2 localizes to kidney cilia and the ciliary level is elevated in orpk mice with polycystic kidney disease. Curr Biol 12, R378–380. [PubMed: 12062067]
3. Yoder BK, Hou X, and Guay-Woodford LM (2002). The polycystic kidney disease proteins, polycystin-1, polycystin-2, polaris, and cystin, are co-localized in renal cilia. J Am Soc Nephrol 13, 2508–2516. [PubMed: 12239239]
4. Ward CJ, Yuan D, Masyuk TV, Wang X, Punyashthiti R, Whelan S, Bacallao R, Torra R, LaRusso NF, Torres VE, et al. (2003). Cellular and subcellular localization of the ARPKD protein; fibrocystin is expressed on primary cilia. Hum Mol Genet 12, 2703–2710. [PubMed: 12925574]
5. Follit JA, Li L, Vucica Y, and Pazour GJ (2010). The cytoplasmic tail of fibrocystin contains a ciliary targeting sequence. J Cell Biol 188, 21–28. [PubMed: 20048263]
6. Li Y, Tian X, Ma M, Jerman S, Kong S, Somlo S, and Sun Z (2016). Deletion of ADP Ribosylation Factor-Like GTPase 13B Leads to Kidney Cysts. J Am Soc Nephrol 27, 3628–3638. [PubMed: 27153923]
7. Seixas C, Choi SY, Polgar N, Umberger NL, East MP, Zuo X, Moreiras H, Ghossoub R, Benmerah A, Kahn RA, et al. (2016). Arl13b and the exocyst interact synergistically in ciliogenesis. Mol Biol Cell 27, 308–320. [PubMed: 26582389]
8. Kleene SJ, and Kleene NK (2017). The native TRPP2-dependent channel of murine renal primary cilia. Am J Physiol Renal Physiol 312, F96–F108. [PubMed: 27760766]
9. Liu X, Vien T, Duan J, Sheu SH, DeCaen PG, and Clapham DE (2018). Polycystin-2 is an essential ion channel subunit in the primary cilium of the renal collecting duct epithelium. Elife 7.
10. Su Q, Hu F, Ge X, Lei J, Yu S, Wang T, Zhou Q, Mei C, and Shi Y (2018). Structure of the human PKD1/PKD2 complex. Science.
11. Chapin HC, and Caplan MJ (2010). The cell biology of polycystic kidney disease. J Cell Biol 191, 701–710. [PubMed: 21079243]
12. Caspary T, Larkins CE, and Anderson KV (2007). The graded response to Sonic Hedgehog depends on cilia architecture. Dev Cell 12, 767–778. [PubMed: 17488627]

13. Gotthardt K, Lokaj M, Koerner C, Falk N, Giessl A, and Wittinghofer A (2015). A G-protein activation cascade from Arl13B to Arl3 and implications for ciliary targeting of lipidated proteins. Elife 4.

14. Ivanova AA, Caspary T, Seyfried NT, Duong DM, West AB, Liu Z, and Kahn RA (2017). Biochemical characterization of purified mammalian ARL13B protein indicates that it is an atypical GTPase and ARL3 guanine nucleotide exchange factor (GEF). J Biol Chem 292, 11091–11108. [PubMed: 28487361]

15. Humbert MC, Weihbrecht K, Searby CC, Li Y, Pope RM, Sheffield VC, and Seo S (2012). ARL13B, PDE6D, and CEP164 form a functional network for INPP5E ciliary targeting. Proc Natl Acad Sci U S A 109, 19691–19696. [PubMed: 23150559]

16. Wright KJ, Baye LM, Olivier-Mason A, Mukhopadhyay S, Sang L, Kwong M, Wang W, Pretorius PR, Sheffield VC, Sengupta P, et al. (2011). An ARL3-UNC119-RP2 GTPase cycle targets myristoylated NPHP3 to the primary cilium. Genes Dev 25, 2347–2360. [PubMed: 22085962]

17. Hakim S, Dyson JM, Feeney SJ, Davies EM, Sriratana A, Koenig MN, Plotnikova OV, Smyth IM, Ricardo SD, Hobbs RM, et al. (2016). Inpp5e suppresses polycystic kidney disease via inhibition of PI3K/Akt-dependent mTORC1 signaling. Hum Mol Genet 25, 2295–2313. [PubMed: 27056978]

18. Cai Y, Fedeles SV, Dong K, Anyatonwu G, Onoe T, Mitobe M, Gao JD, Okuhara D, Tian X, Gallagher AR, et al. (2014). Altered trafficking and stability of polycystins underlie polycystic kidney disease. J Clin Invest 124, 5129–5144. [PubMed: 25365220]

19. Gainullin VG, Hopp K, Ward CJ, Hommerding CJ, and Harris PC (2015). Polycystin-1 maturation requires polycystin-2 in a dose-dependent manner. J Clin Invest 125, 607–620. [PubMed: 25574838]

20. Kim H, Xu H, Yao Q, Li W, Huang Q, Outeda P, Cebotaru V, Chiaravalli M, Boletta A, Piontek K, et al. (2014). Ciliary membrane proteins traffic through the Golgi via a Rabep1/GGA1/Arl3-dependent mechanism. Nat Commun 5, 5482. [PubMed: 25405894]

21. Hogan MC, Manganelli L, Woollard JR, Masyuk AI, Masyuk TV, Tammachote R, Huang BQ, Leontovich AA, Beito TG, Madden BJ, et al. (2009). Characterization of PKD protein-positive exosome-like vesicles. J Am Soc Nephrol 20, 278–288. [PubMed: 19158352]

22. Pisitkun T, Shen RF, and Knepper MA (2004). Identification and proteomic profiling of exosomes in human urine. Proc Natl Acad Sci U S A 101, 13368–13373. [PubMed: 15326289]

23. Yu S, Hackmann K, Gao J, He X, Piontek K, Garcia-Gonzalez MA, Menezes LF, Xu H, Germino GG, Zuo J, et al. (2007). Essential role of cleavage of Polycystin-1 at G protein-coupled receptor proteolytic site for kidney tubular structure. Proc Natl Acad Sci U S A 104, 18688–18693. [PubMed: 18003909]

24. Yoshiba S, Shiratori H, Kuo IY, Kawasumi A, Shinohara K, Nonaka S, Asai Y, Sasaki G, Belo JA, Sasaki H, et al. (2012). Cilia at the node of mouse embryos sense fluid flow for left-right determination via Pkd2. Science 338, 226–231. [PubMed: 22983710]

25. Field S, Riley KL, Grimes DT, Hilton H, Simon M, Powles-Glover N, Siggers P, Bogani D, Greenfield A, and Norris DP (2011). Pkd1l1 establishes left-right asymmetry and physically interacts with Pkd2. Development 138, 1131–1142. [PubMed: 21307093]

26. Lin F, Hiesberger T, Cordes K, Sinclair AM, Goldstein LS, Somlo S, and Igarashi P (2003). Kidney-specific inactivation of the KIF3A subunit of kinesin-II inhibits renal ciliogenesis and produces polycystic kidney disease. Proc Natl Acad Sci U S A 100, 5286–5291. [PubMed: 12672950]

27. Ma M, Tian X, Igarashi P, Pazour GJ, and Somlo S (2013). Loss of cilia suppresses cyst growth in genetic models of autosomal dominant polycystic kidney disease. Nat Genet 45, 1004–1012. [PubMed: 23892607]

28. Shibazaki S, Yu Z, Nishio S, Tian X, Thomson RB, Mitobe M, Louvi A, Velazquez H, Ishibe S, Cantley LG, et al. (2008). Cyst formation and activation of the extracellular regulated kinase pathway after kidney specific inactivation of Pkd1. Hum Mol Genet 17, 1505–1516. [PubMed: 18263604]

29. Davenport JR, Watts AJ, Roper VC, Croyle MJ, van Groen T, Wyss JM, Nagy TR, Kesterson RA, and Yoder BK (2007). Disruption of intraflagellar transport in adult mice leads to obesity and slow-onset cystic kidney disease. Curr Biol 17, 1586–1594. [PubMed: 17825558]
30. Patel V, Li L, Cobo-Stark P, Shao X, Somlo S, Lin F, and Igarashi P (2008). Acute kidney injury and aberrant planar cell polarity induce cyst formation in mice lacking renal cilia. Hum Mol Genet 17, 1578–1590. [PubMed: 18263895]
31. Piontek K, Menezes LF, Garcia-Gonzalez MA, Huso DL, and Germino GG (2007). A critical developmental switch defines the kinetics of kidney cyst formation after loss of Pkd1. Nat Med 13, 1490–1495. [PubMed: 17965720]
32. Mukhopadhyay S, Wen X, Chih B, Nelson CD, Lane WS, Scales SJ, and Jackson PK (2010). TULP3 bridges the IFT-A complex and membrane phosphoinositides to promote trafficking of G protein-coupled receptors into primary cilia. Genes Dev 24, 2180–2193. [PubMed: 20889716]
33. Badgandi HB, Hwang SH, Shimada IS, Loriot E, and Mukhopadhyay S (2017). Tubby family proteins are adapters for ciliary trafficking of integral membrane proteins. J Cell Biol 216, 743–760. [PubMed: 28154160]
34. Yu J, Carroll TJ, and McMahon AP (2002). Sonic hedgehog regulates proliferation and differentiation of mesenchymal cells in the mouse metanephric kidney. Development 129, 5301–5312. [PubMed: 12399320]
35. Shao X, Somlo S, and Igarashi P (2002). Epithelial-specific Cre/lox recombination in the developing kidney and genitourinary tract. J Am Soc Nephrol 13, 1837–1846. [PubMed: 12089379]
36. Shillingford JM, Piontek KB, Germino GG, and Weimbs T (2010). Rapamycin ameliorates PKD resulting from conditional inactivation of Pkd1. J Am Soc Nephrol 21, 489–497. [PubMed: 20075061]
37. Shillingford JM, Murcia NS, Larson CH, Low SH, Hedgepeth R, Brown N, Flask CA, Novick AC, Goldfarb DA, Kramer-Zucker A, et al. (2006). The mTOR pathway is regulated by polycystin-1, and its inhibition reverses renal cystogenesis in polycystic kidney disease. Proceedings of the National Academy of Sciences of the United States of America 103, 5466–5471. [PubMed: 16567633]
38. Wang Q, Cobo-Stark P, Patel V, Somlo S, Han PL, and Igarashi P (2018). Adenylyl cyclase 5 deficiency reduces renal cyclic AMP and cyst growth in an orthologous mouse model of polycystic kidney disease. Kidney international 93, 403–415. [PubMed: 29042084]
39. Choi YH, Suzuki A, Hajarnis S, Ma Z, Chapin HC, Caplan MJ, Pontoglio M, Somlo S, and Igarashi P (2011). Polycystin-2 and phosphodiesterase 4C are components of a ciliary A-kinase anchoring protein complex that is disrupted in cystic kidney diseases. Proc Natl Acad Sci U S A 108, 10679–10684. [PubMed: 21670265]
40. Torres VE, Wang X, Qian Q, Somlo S, Harris PC, and Gattone VH, 2nd (2004). Effective treatment of an orthologous model of autosomal dominant polycystic kidney disease. Nature medicine 10, 363–364.
41. Mukhopadhyay S, Wen X, Ratti N, Loktev A, Rangell L, Scales SJ, and Jackson PK (2013). The ciliary G-protein-coupled receptor Gpr161 negatively regulates the Sonic hedgehog pathway via cAMP signaling. Cell 152, 210–223. [PubMed: 23332756]
42. Faust D, Geelhaar A, Eisermann B, Eichhorst J, Wiesner B, Rosenthal W, and Klussmann E (2013). Culturing primary rat inner medullary collecting duct cells. Journal of visualized experiments : JoVE.
43. Geng L, Okuhara D, Yu Z, Tian X, Cai Y, Shibazaki S, and Somlo S (2006). Polycystin-2 traffics to cilia independently of polycystin-1 by using an N-terminal RVxP motif. J Cell Sci 119, 1383–1395. [PubMed: 16537653]
44. Qian F, Germino FJ, Cai Y, Zhang X, Somlo S, and Germino GG (1997). PKD1 interacts with PKD2 through a probable coiled-coil domain. Nat Genet 16, 179–183. [PubMed: 9171830]
45. Roux KJ, Kim DI, Raida M, and Burke B (2012). A promiscuous biotin ligase fusion protein identifies proximal and interacting proteins in mammalian cells. The Journal of cell biology 196, 801–810. [PubMed: 22412018]

46. Norman RX, Ko HW, Huang V, Eun CM, Abler LL, Zhang Z, Sun X, and Eggenschwiler JT (2009). Tubby-like protein 3 (TULP3) regulates patterning in the mouse embryo through inhibition of Hedgehog signaling. Hum Mol Genet 18, 1740–1754. [PubMed: 19286674]

47. Santagata S, Boggon TJ, Baird CL, Gomez CA, Zhao J, Shan WS, Myszka DG, and Shapiro L (2001). G-protein signaling through tubby proteins. Science 292, 2041–2050. [PubMed: 11375483]

48. Jonassen JA, SanAgustin J, Baker SP, and Pazour GJ (2012). Disruption of IFT complex A causes cystic kidneys without mitotic spindle misorientation. J Am Soc Nephrol 23, 641–651. [PubMed: 22282595]

49. Jonassen JA, San Agustin J, Follit JA, and Pazour GJ (2008). Deletion of IFT20 in the mouse kidney causes misorientation of the mitotic spindle and cystic kidney disease. J Cell Biol 183, 377–384. [PubMed: 18981227]

50. Schrick JJ, Vogel P, Abuin A, Hampton B, and Rice DS (2006). ADP-ribosylation factor-like 3 is involved in kidney and photoreceptor development. Am J Pathol 168, 1288–1298. [PubMed: 16565502]

51. Ma M, Gallagher AR, and Somlo S (2017). Ciliary Mechanisms of Cyst Formation in Polycystic Kidney Disease. Cold Spring Harb Perspect Biol.

52. Bergmann C, Fliegauf M, Bruchle NO, Frank V, Olbrich H, Kirschner J, Schermer B, Schmedding I, Kispert A, Kranzlin B, et al. (2008). Loss of nephrocystin-3 function can cause embryonic lethality, Meckel-Gruber-like syndrome, situs inversus, and renal-hepatic-pancreatic dysplasia. Am J Hum Genet 82, 959–970. [PubMed: 18371931]

53. Hwang SH, White KA, Somatilaka BN, Shelton JM, Richardson JA, and Mukhopadhyay S (2018). The G protein-coupled receptor Gpr161 regulates forelimb formation, limb patterning and skeletal morphogenesis in a primary cilium-dependent manner. Development 145.

54. Shimada IS, Hwang SH, Somatilaka BN, Wang X, Skowron P, Kim J, Kim M, Shelton JM, Rajaram V, Xuan Z, et al. (2018). Basal Suppression of the Sonic Hedgehog Pathway by the G-Protein-Coupled Receptor Gpr161 Restricts Medulloblastoma Pathogenesis. Cell Rep 22, 1169–1184. [PubMed: 29386106]

55. Pal K, Badgandi H, and Mukhopadhyay S (2015). Studying G protein-coupled receptors: immunoblotting, immunoprecipitation, phosphorylation, surface labeling, and cross-linking protocols. Methods Cell Biol 127, 303–322. [PubMed: 25837398]

Highlights

- Nephron-specific *Tulp3* knockouts develop cystic kidneys without disrupting cilia.
- Cystogenesis is intermediate between that caused by loss of polycystin-1 or cilia.
- Polycystin-2 and Arl13b are reduced in cilia of knockout collecting duct cells.
- Arl13b is the likely polycystin-independent ciliary factor repressing cystogenesis.

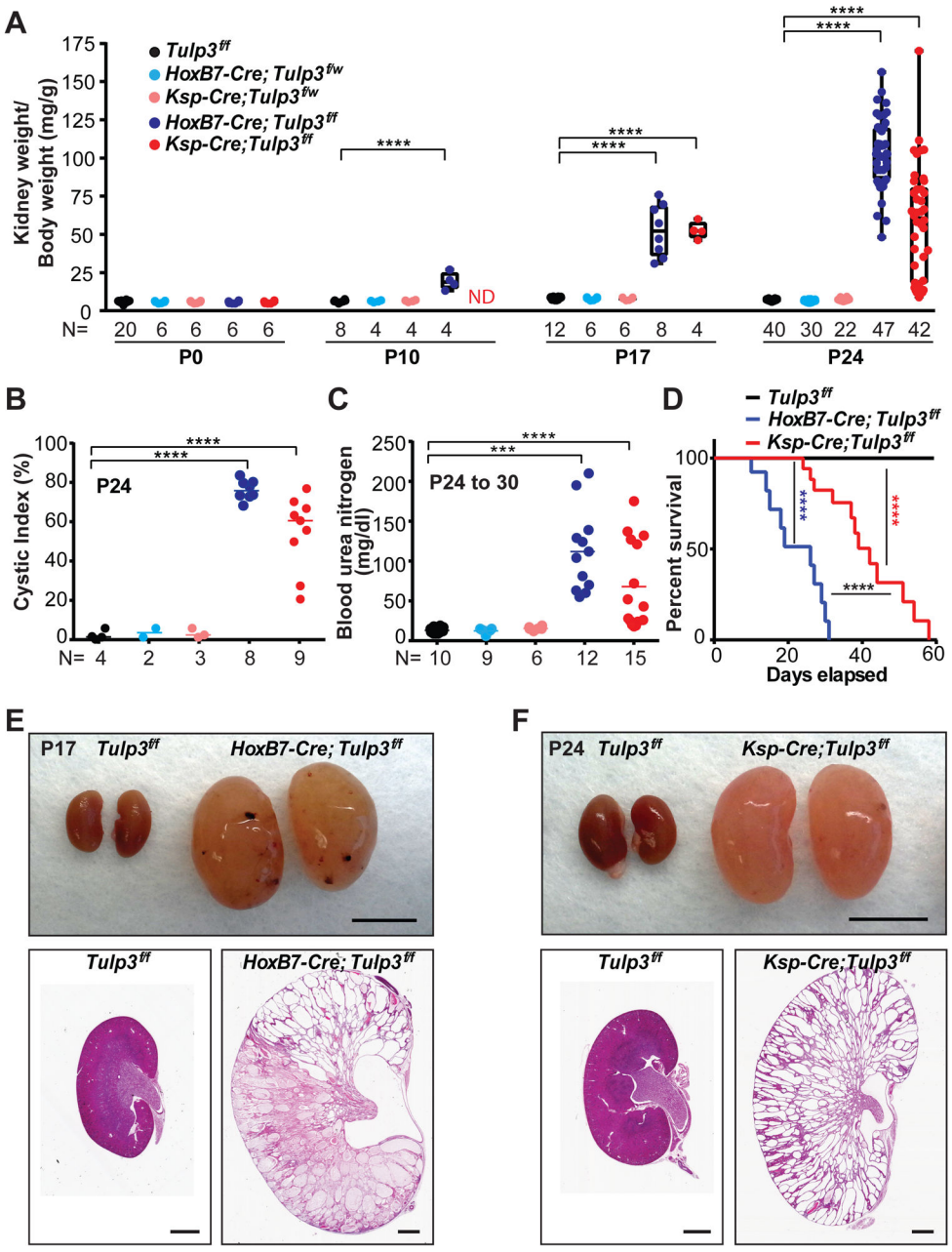

Figure 1. Lack of *Tulp3* causes cystic kidney disease.

(A) Kidney to body weight ratios in *HoxB7-Tulp3* cko (*HoxB7-Cre; Tulp3*$^{f/f}$) and *Ksp-Tulp3* cko (*Ksp-Cre; Tulp3*$^{f/f}$) mice. Significant increase in cko is evident as early as P10. **** P<0.0001 by one-way ANOVA analysis, box-and-whisker plots.

(B) Significantly increased cystic index in *Tulp3* cko. ****, P<0.0001 by t-test.

(C) Significantly increased BUN in *Tulp3* cko. ***, P<0.001; ****, P<0.0001 by t-test. Each dot color-coded as in **(A, C)** represents data from separate mice, or kidneys from separate mice (N, mentioned below charts) **(B)**. Horizontal bars show mean (**B, C**).

(D) Kaplan-Meier survival curves of control (N=36), *HoxB7-Tulp3* cko (N=10) and *Ksp-Tulp3* cko (N=18) mice. ****, P<0.0001 by log-rank test.

(E-F) Histological analysis suggested that both *Tulp3* cko models had extensive cysts at P17-24 throughout the tissue with little remaining parenchyma (multiple kidneys shown in Figure S1D). Each dot represents data from a separate mouse or kidney. Scale, 1 cm (top) and 1 mm (bottom). See also Figure S1.

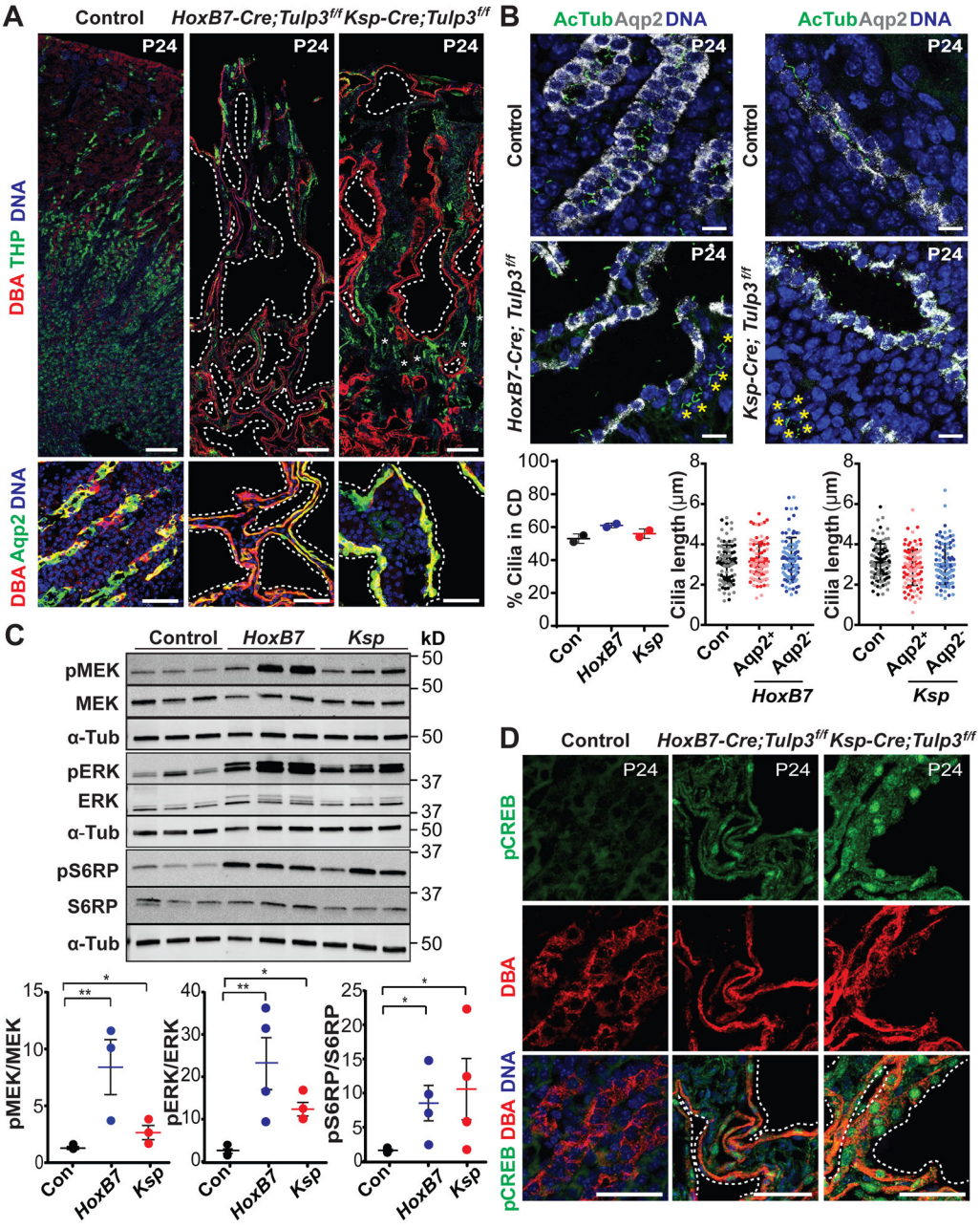

Figure 2. Intact cilia with upregulation of multiple signaling pathways in *Tulp3* cko.

(A) DBA/Aqp2 or DBA/THP co-staining in *Tulp3* cko kidney sections at P24. DBA/Aqp2 positive cyst linings are marked by broken lines. Asterisks mark a few small THP positive cysts. N=2/genotype.

(B) Kidney sections at P24 counterstained with Aqp2 and acetylated tubulin (AcTub). Cilia are unaffected in *Tulp3* cko models in Aqp2-positive collecting duct (CD) or cysts. Yellow asterisks mark cilia in Aqp2 negative renal segments. Data shown as mean ± SD. Quantification of % ciliated Aqp2+ cells from two mice each in both cortical and medullary regions are shown (bottom left, total cells counted/genotype >390). Quantification of length

of >100 cilia/mouse (each mouse with different shades) is shown bottom right. ***, P<0.001; ****, P<0.0001 by t-test.

(C) pMEK, MEK, pERK, ERK, pS6RP and S6RP immunoblotting at P24. Ratios of individual phosphoprotein to total protein, each normalized to α-Tubulin separately, is shown below. N=3-4 each condition. * P<0.05, ** P<0.01.

(D) pCREB immunostaining shows upregulated nuclear levels in DBA-positive collecting duct/cyst linings (broken lines) in kidney sections of *Tulp3* cko models at P24 (N=2 each). Control littermates: *Tulp3*$^{f/+}$(**A, B** left column), *Ksp-Cre;Tulp3*$^{f/+}$ (**B** right column), *HoxB7-Cre; Tulp3*$^{f/+}$(**D**). Abbreviations: Con, control littermate; *HoxB7, HoxB7-Tulp3* cko; *Ksp, Ksp-Tulp3* cko. Scale: A, 200 μm; B, D, 50 μm. See also Figure S2.

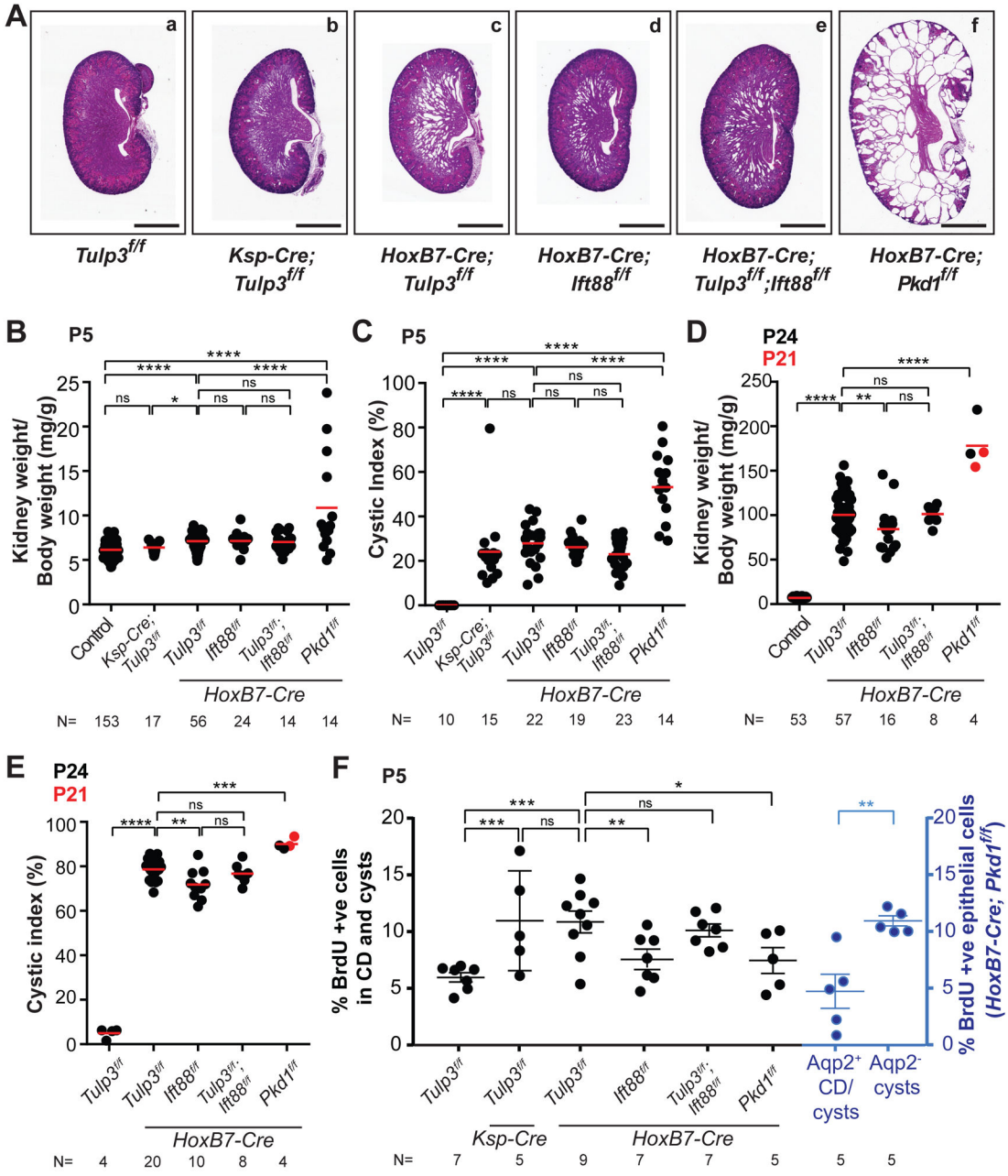

Figure 3. Cystogenesis in *Tulp3* cko is less severe than upon *Pkd1* deletion.

(A) (a-f) Cysts in both *Tulp3* cko models were apparent at P5, mostly affecting medulla, although some cortical cysts were also seen. *Pkd1* cko cysts were both cortical and medullary and larger in size. *Tulp3/Ift88* double cko mostly had medullary cysts, similar to *Tulp3* cko.

(B-E) Kidney to body weight ratios, and cystic indices at P5 (B-C) and P21-P24 (D-E). *Pkd1* cko animals had significantly higher cystic index than *Tulp3* or *Ift88* cko kidneys at P5. *Tulp3* cko animals had cystic index intermediate between that of *Pkd1* and *Ift88* cko kidneys at P24. Horizontal bars, mean. Control, $Tulp3^{f/f}$ or $Tulp3^{f/+}$ not expressing *Cre.*

(F) Increased proliferation in cystic kidneys in *Tulp3* cko with respect to loss of cilia. BrdU positive cells in collecting duct (CD) epithelia from tubules (marked by Aqp2) or cysts at P5. Many of the cysts in *Pkd1* cko were lined by squamoid cells without Aqp2 immunostaining (marked by yellow asterisks, Figure S3C), with quantification shown in blue (right panel). Data shown as mean ± SEM (**F**).

Each dot represents data from a separate mouse or kidney (N, mentioned below charts) (**B-E**). Total number of cells counted, 4000-10000/kidney (**F**). *, P<0.05; **, P<0.01; ***, P<0.001; ****, P<0.0001 by one-way ANOVA with Sidak's multiple comparisons tests (**B-F**), except $Aqp^{+/-}$ comparison (blue, **F**) by t-test. Scale: A, 1 mm. See also Figure S3.

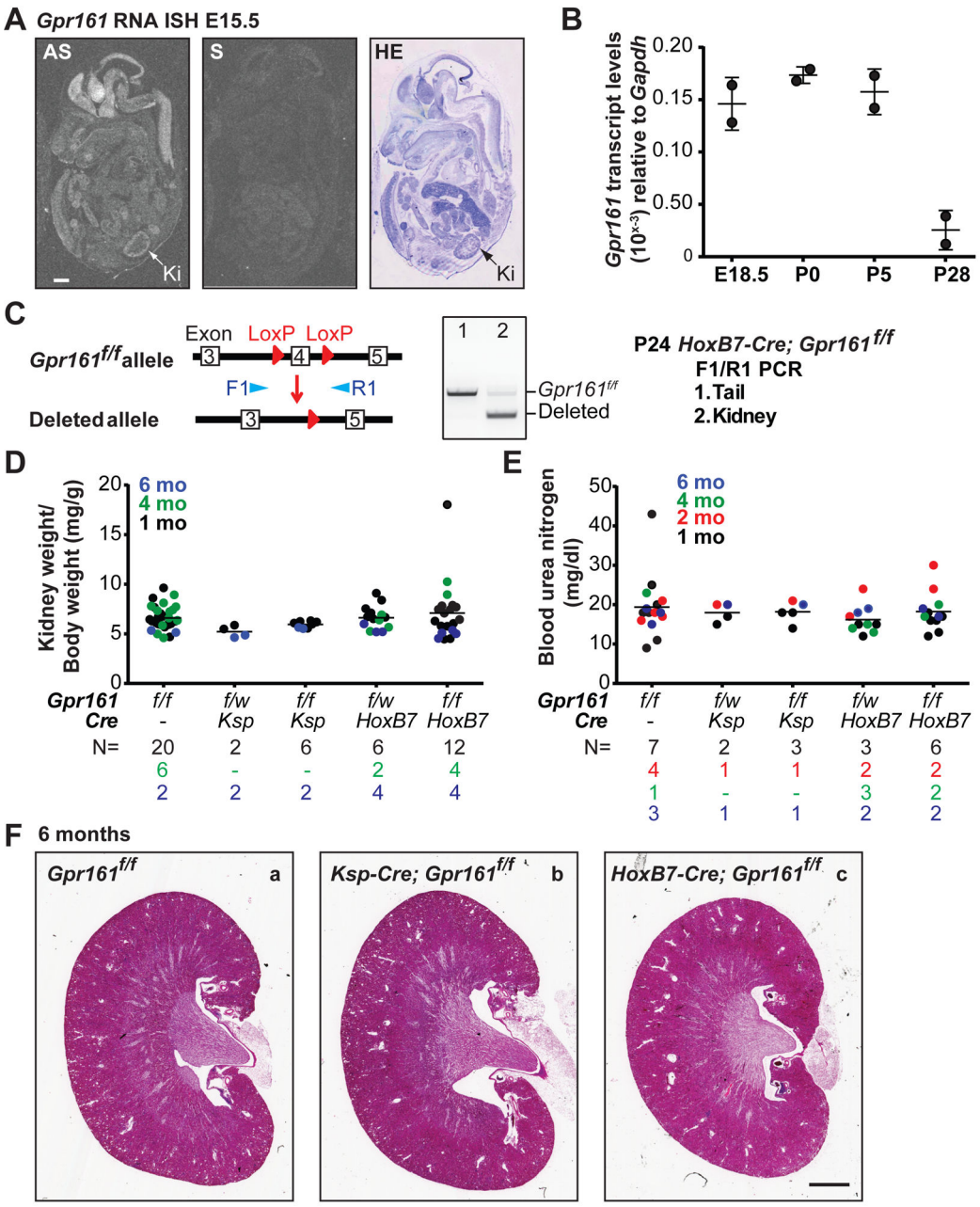

Figure 4. Lack of *Gpr161* does not cause cystic kidney disease.

(A) Radioisotopic RNA *in situ* hybridization (ISH) using *Gpr161* anti-sense (AS) or sense (S) probe in E15.5 sagittal sections shows transcript expression in kidney (Ki). HE refers to hematoxylin eosin stained section.

(B) Transcript levels of *Gpr161* in wild type kidneys using qRT-PCR.

(C) Targeting strategy for *Gpr161* conditional knockouts and genotyping.

(D) Kidney to body weight ratios in *Gpr161* cko mouse.

(E) BUN levels in *Gpr161* cko. Each dot represents data from a separate kidney (**D**) or a mouse (**E**) (N, mentioned below charts).

(F) Images of kidneys from control littermates, *HoxB7-Gpr161* cko and *Ksp-Gpr161* cko mice at 2 months. Scale: A and F, 1 mm. See also Figure S4.

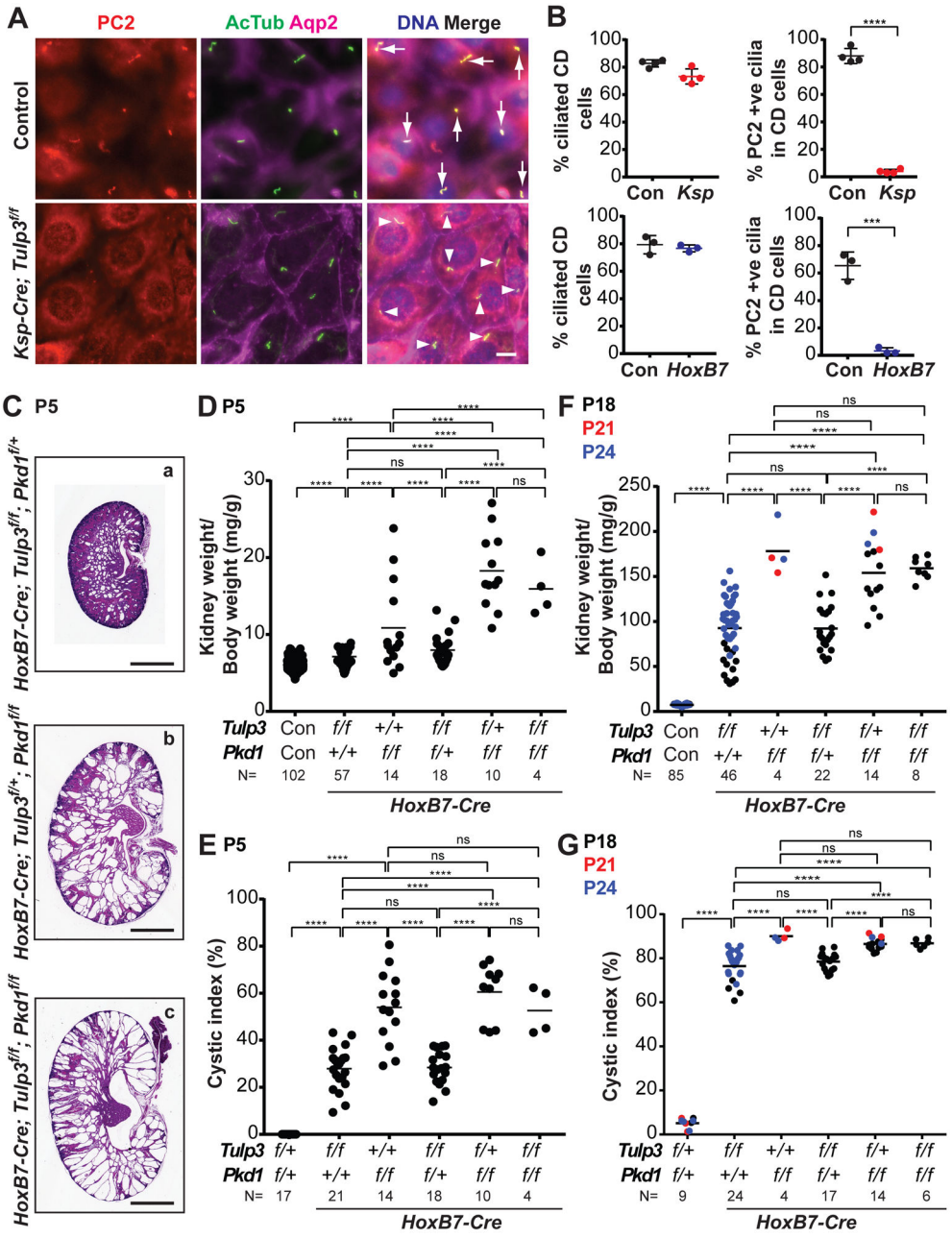

Figure 5. Concomitant loss of *Tulp3* does not inhibit cystogenesis from *Pkd1* loss.

(A) Primary IMCD cells cultured from control or *Ksp-Tulp3* cko kidneys at P20, counterstained with PC2, Aqp2, and acetylated tubulin (AcTub). PC2 trafficking to cilia are reduced in *Ksp-Tulp3* cko cells. Arrows and arrowheads point to PC2 positive and negative cilia, respectively. Aqp2 positive cells ranged from 81-97%.

(B) Primary IMCD cells were cultured from littermate control or *Ksp-Tulp3* cko kidneys at P20, and littermate control or *HoxB7-Tulp3* cko kidneys at P16, and processed for immunofluorescence as in (A). Data shown as mean ± SD. Images from *HoxB7-Tulp3* cko cells are shown in Figure S5A. Control (Con), P20; *Ksp, Ksp-Tulp3* cko, N=4 mice/ genotype and total cells counted >700/genotype. Control (Con), P16; *HoxB7, HoxB7-Tulp3*

cko, N=3 mice/genotype, and total cells counted >270/genotype. *Tulp3* transcript levels in cko were reduced compared to controls (Control, 1.06 ± 0.07 (N=4) and *Ksp*, 0.03 ± 0.01 (N=4); Control, 0.92 ±0.13 (N=3) and *HoxB7,* 0 ± 0 (N=3)).

(C) Cysts in designated backgrounds at P5. Compare with P5 data in Figure 3A.

(D-G) Kidney to body weight ratios, and cystic indices at P5 (**D, E**) and P18-P24 (**F, G**). Con (**D, F**): *f/f* or *f/+* for either *Tulp3* or *Pkd1.* Data of *HoxB7-Pkd* cko same as in Figure 3B-E and shown here again for comparison purposes.

Each dot represents data from a separate mouse or kidney (**B, D-G**) (N, mentioned below charts). *, P<0.05; **, P<0.01; ***, P<0.001; ****, P<0.0001 by one-way ANOVA with Sidak's multiple comparisons tests (**D-G**) or t-test (**B**). Scale: A, 10 μM; C, 1 mm. See also Figure S5.

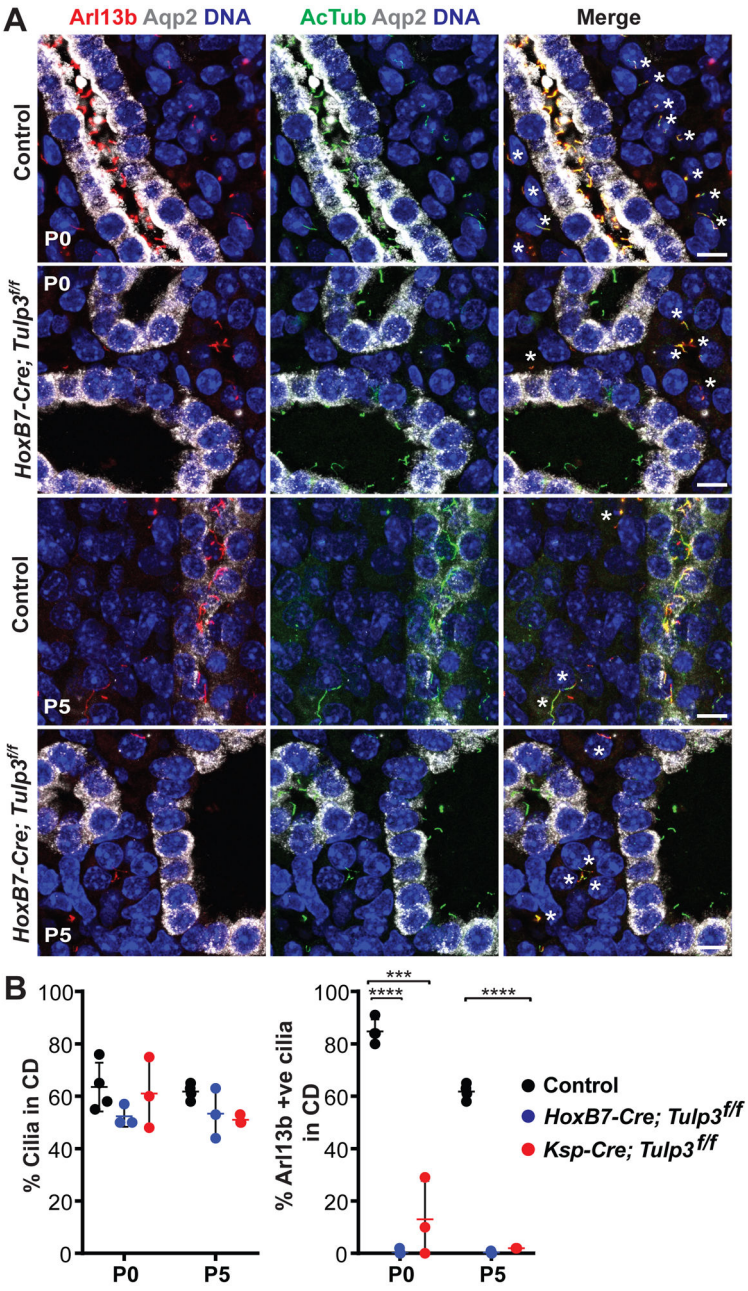

Figure 6. Defect in trafficking of Arl13b to cilia precedes cyst formation in *Tulp3* cko.

(A) Kidney sections from control or *HoxB7-Cre; Tulp3* cko mice at designated ages, counterstained with Aqp2, acetylated tubulin (AcTub), and Arl13b. Cilia are unaffected in *Tulp3* cko models in Aqp2-positive collecting duct/cysts. Arl13b trafficking to cilia is affected by P0. Asterisks mark Aqp2-negative nephron segments retaining Arl13b-positive cilia. Control littermates: $Tulp3^{f/f}$ at P0 and $Tulp3^{f/+}$ at P5. Scale, 50 μm.

(**B)** Quantification from mice (N=2-3) per time point and genotype in both cortical and medullary regions. Total cells counted, >550-1100/genotype and time point. ***, P<0.001; ****, P<0.0001 by t-test. Error bars represent SEM. See also Figure S6.

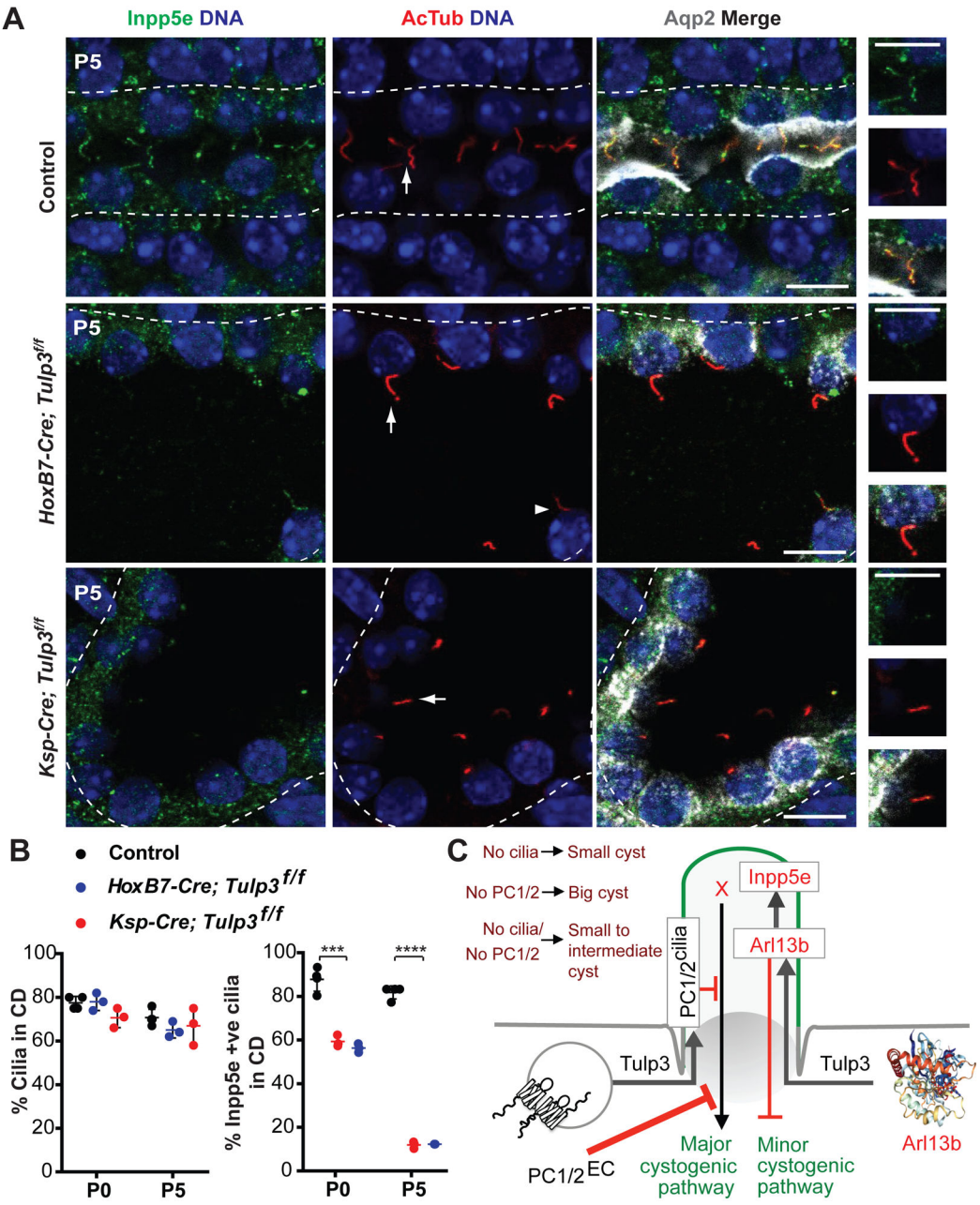

Figure 7. Defective trafficking of Arl13b-regulated lipidated cargo Inpp5e in *Tulp3* cko.

(A) Kidney sections from control (*Tulp3*$^{f/f}$), *HoxB7-Tulp3* cko and *Ksp-Tulp3* cko mice at P5, counterstained with Aqp2, acetylated tubulin (AcTub), and Inpp5e. White dashed lines mark the Aqp2-positive collecting duct/cyst areas. Aqp2-positive collecting ducts/cysts (white dashed lines) are positive for Inpp5e positive cilia, but cysts in *HoxB7-Tulp3* cko and *Ksp-Tulp3* cko start to lose ciliary trafficking by P5. Arrows point to cilia shown in high magnification in the rightmost panels. Arrowhead point to an Inpp5e positive cilium in *HoxB7-Tulp3* cko. Scale, 10 μm.

(B) Quantification of staining shown as in **(A)**. Control (N=4) or *HoxB7-Tulp3* cko (N=3) and *Ksp-Tulp3* cko (N=3) mice at P0 and P5. Total cells counted, >740/genotype and time point. ***, P<0.001; ****, P<0.0001 by t-test. Error bars represent SEM.

(C) Cartoon summarizing implications of the current results with respect to the role of proposed cilia-dependent positive and negative cystogenic regulators. Abbreviations: EC, extra-ciliary. See also Figure S7.